ACS NANO
Cite This: ACS Nano 2018, 12, 7855−7865
www.acsnano.org

ARTICLE

Invariance of Water Permeance through Size-Differentiated Graphene Oxide Laminates

Vivek Saraswat,[†] Robert M. Jacobberger,[†] Joshua S. Ostrander,[‡] Courtney L. Hummell,[†] Austin J. Way,[†] Jialiang Wang,[†] Martin T. Zanni,[‡] and Michael S. Arnold*[,†]

[†]Department of Materials Science & Engineering, University of Wisconsin—Madison, Madison, Wisconsin 53706, United States
[‡]Department of Chemistry, University of Wisconsin—Madison, Madison, Wisconsin 53706, United States

Supporting Information

ABSTRACT: Laminates made of graphene oxide nanosheets have been shown to exhibit high water permeance and salt rejection and, therefore, have generated immense interest from the scientific community due to their potential in separation applications. However, there is no clear consensus on the water-transport pathways through such laminates. In this study, we synthesized chemically identical graphene oxide nanosheets with 2 orders of magnitude difference in lateral sizes and measured water permeance through laminates of different thicknesses fabricated by pressure-assisted deposition of these nanosheets. Our results reveal that water permeance through these laminates is nearly the same despite such massive difference in lateral sheet size. Furthermore, we simulated fluid flow through laminates using an interconnected nanochannel network model for comparison with experiments. The simulations in combination with the experimental data show that it is unlikely that the dominant fluid transport pathway is a circuitous, lateral pathway around individual sheets, as has been proposed in some studies. Rather, nonideal factors including trans-sheet flow through pinhole defects in sheet interiors and/or flow-through regions arising from imperfect stacking in the laminates can significantly affect the fluid transport pathways. The presence of such nonidealities is also supported by thickness- and time-dependent measurements of permeance and by infrared spectroscopy, which indicates that water predominantly adopts a bulk-like structure in the laminates. These analyses are significant steps toward understanding water transport through graphene oxide laminates and provide further insight toward the structure of water inside these materials, which could have immense potential in next-generation separation applications.

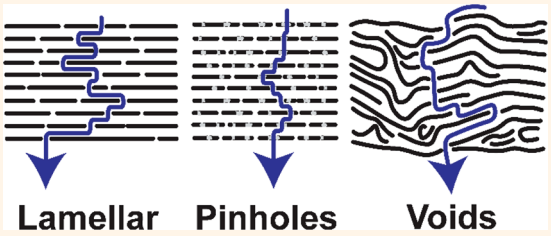

KEYWORDS: *graphene oxide laminates, water transport mechanisms, two-dimensional materials, infrared spectroscopy, nanoconfined water*

Laminates of graphene oxide (GO) have recently emerged as promising materials for gas and liquid phase chemical separation membranes[1,2] because of their inexpensive synthesis,[3] tunable selectivity,[4] high permeance,[5] and scalable fabrication.[6] In these laminates, the flow of molecules and ions is believed to be confined in ultrathin channels that are bounded by layered sheets of GO. When dry, the channel gap is too narrow to permit even the flow of atomic He.[7] However, the laminates swell when hydrated, permitting water transport[8,9] in which Na^+, Cl^-, and other ions can be rejected by tuning the interlayer spacing of the laminates through control over the level of their hydration.[4] Due to these attributes, GO laminates are being pursued for cost-effective water purification, treatment, and desalination technologies.[10]

Despite the technological interest in GO laminates, a clear understanding of the factors that dictate water transport within the layers and the microstructure of these materials does not yet exist.[11] One hypothesis is that the flow of water within the laminates follows a circuitous pathway around individual GO sheets in which water must first flow laterally over considerable distance to the edges of sheets before progressing deeper within the laminates. In order to reconcile measurements of high water permeance with the long, circuitous pathway that water must follow in this scenario, it has been surmised that smooth, hydrophobic, unoxidized, graphene-like regions within GO must exist within the laminates that form interconnected nanocapillaries that promote nearly frictionless flow. It has also been proposed that water adopts an ordered, two-dimensional structure within these nanocapillaries.[7]

This circuitous pathway/nanocapillary hypothesis has been disputed.[12] High-resolution transmission electron microscopy (HR-TEM) studies have shown that pristine regions of unoxidized graphene within typical GO samples are rather

Received: March 17, 2018
Accepted: July 11, 2018
Published: July 11, 2018

DOI: 10.1021/acsnano.8b02015
ACS Nano 2018, 12, 7855−7865

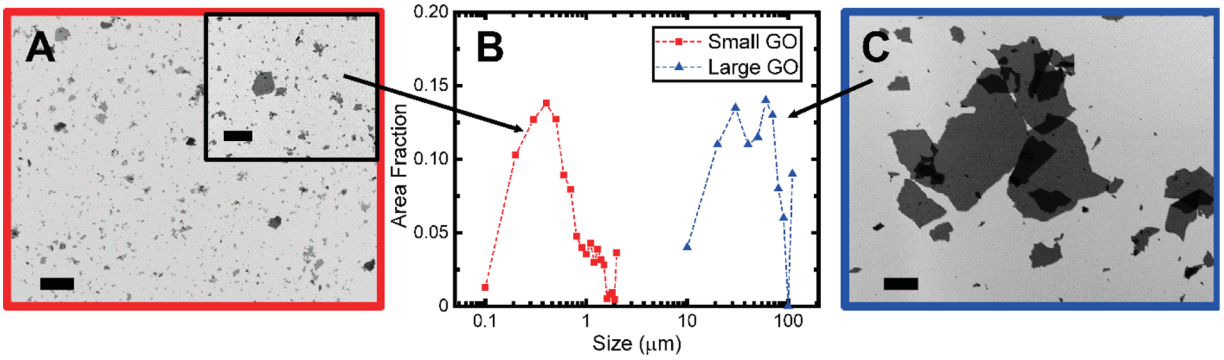

Figure 1. SEM images of (A) Small and (C) Large GO spin-cast onto SiO_2. (B) Area fraction *versus* lateral size distributions of these sheets. Scale bars in A, A inset, and C are 10, 5, and 10 μm, respectively.

isolated, accounting for only 16% of the total area.[13−15] Raman spectroscopy studies have likewise indicated that clusters of sp^2 carbon smaller than 2−3 nm are isolated within the sp^3 C−O matrix.[15,16] Thus, the presence of interconnected unoxidized graphene nanocapillaries is unlikely. The electrically insulating nature of GO[17] also confirms that unoxidized graphene domains are unlikely to be well interconnected. Moreover, according to the nanocapillary hypothesis,[4,7,8] the interlayer spacing of hydrophobic capillaries in dried GO laminates is ∼7 Å, which should provide a 3.5 Å wide channel that is large enough to permeate He, H_2, and CO_2 with kinetic diameters of 2.6, 2.9, and 3.3 Å, respectively.[18,19] However, this expectation is inconsistent with the absence of He permeation observed by Nair *et al.*[7] Even if graphene-like hydrophobic nanocapillaries do exist, Wei *et al.*[20] have predicted using MD simulations that ultrafast water flow within the nanocapillaries should nonetheless be slowed due to side-pinning effects, and Devanathan *et al.*[11] have likewise predicted that water transport through GO laminates should be slowed by strong hydrogen-bonding interactions with oxygen-rich functional groups in the GO, in which the water adopts a bulk-like structure.

Considering these inconsistencies of the circuitous pathway/nanocapillary hypothesis, several nonidealities and alternative hypotheses have been proposed. Of particular significance are the roles of (1) pinhole defects in sheet interiors and (2) imperfect sheet packing. With regard to (1), it has been hypothesized that pinhole defects can provide a route for trans-sheet flow.[11−13] At a sufficiently high density of pinhole defects, the long, lateral flow of fluid around each sheet can be avoided, resulting in a much shorter path-length for permeation. HR-TEM studies have confirmed the presence of nanometer-scale, pore-like defects in isolated sheets of GO, giving support to this hypothesis.[13,21] (2) Another possibility is that imperfect stacking in the laminates can lead to new fluid transport pathways. This is conceivable because the ideal lamellar stacking of sheets—as assumed in the nanocapillary hypothesis—is unlikely to occur in an actual pressure or vacuum assisted deposition, resulting in voids, wrinkles, and a disordered microstructure. These features could provide alternative pathways for fluid flow including the possibility that water might transverse around multiple sheets at a time,[19,22,23] resulting in a higher effective permeance.

In this study, we seek to further understand the mechanism of water transport inside GO laminates. Primarily, does water travel the entire lateral dimension of individual GO nanosheets in confined hydrophobic graphene capillaries or do the presence of pinhole defects and imperfect stacking of sheets provide a shorter pathway for water transport? To answer this question, we synthesized size-controlled GO nanosheets *via* a modified Hummers process[24,25] and compared water permeance through laminates of various thicknesses formed by the pressure-assisted deposition of these nanosheets. These nanosheets were found to be chemically similar, which was confirmed by X-ray photoelectron spectroscopy (XPS) and Fourier transform infrared spectroscopy (FTIR). Our results show that the ratio of water permeances of these laminates varies between 1.4−2.5 for applied pressures between 1−5 bar despite 2 orders of magnitude difference in lateral sheet sizes. Additionally, we modeled water transport through laminates using an interconnected nanochannel network model for comparison with experiments. To understand the predominant configuration (confined or bulk-like) of water inside the GO laminates, we hydrated 250 nm thick GO laminates with 10% D_2O. By characterizing the O−D stretch in FTIR spectra, we conclude that water intercalated in GO laminates primarily exhibits bulk-like behavior. Analysis of size-dependent permeance data (in addition to thickness- and time-dependent data) in conjunction with the simulations and FTIR spectra shows that it is unlikely that the dominant fluid transport pathway is a circuitous, lateral pathway around individual sheets. Rather, fluid flow is likely dictated by two structural features: (1) pinhole defects in sheet interiors that circumvent the necessity to traverse around the entire sheet length and/or (2) imperfect stacking and incomplete compression of GO laminates that provide "short-cuts" for water to permeate without having to flow between the individual layers.

RESULTS AND DISCUSSION

Synthesis of Small and Large GO Sheets. We used the modified Hummers' method to synthesize the GO sheets.[25,26] Using this method, H_2SO_4 acts as a graphite intercalation compound that helps exfoliate graphite into individual graphene monolayers.[27] $KMnO_4$ on reaction with H_2SO_4 provides dimanganese heptoxide (Mn_2O_7) that acts as an oxidizing species[28] and imparts oxygen-rich functional groups to graphene monolayers. H_2O_2 aids in removal of excess permanganate contamination.[29] The last step is the washing of GO with water to remove the acid and the oxidizing agents until a constant pH level is attained. The removal of the residual acid was also confirmed *via* XPS, in which sulfate ions were detected at an abundance of <1% (Figure S7). While the exact structure of GO is still not clear,[28] the model proposed by Lerf[30] and Klinowski[31] is a widely accepted one. In this model, GO is treated as a graphene sheet decorated with

DOI: 10.1021/acsnano.8b02015
ACS Nano 2018, 12, 7855−7865

epoxides and hydroxyls in the basal plane and carboxylic acids and hydroxyls on the edges.

It is believed that size of the GO sheets depends on size of the starting graphite flakes and the processing conditions used during synthesis.[32] We used two different approaches involving subtle changes to the modified Hummers' method to synthesize GO sheets with vastly different lateral sizes as opposed to using ultrasonication to control sheet size, which can undesirably introduce additional pinhole defects, enlarge existing defects, and further oxidize the sheets.[33] In the first variant of the Hummer's method, we synthesized GO sheets with lateral sizes predominantly <1 μm (hereafter referred to as Small GO), and using the second method, we synthesized GO sheets with lateral sizes ranging from 10−100 μm (hereafter referred to as Large GO). Complete details of the synthesis procedure for these two sheets can be found in the methods section. The graphite source for both Small GO and Large GO was the same.

Characterization of Small and Large GO Sheets. Figure 1 shows SEM images of Small and Large GO sheets along with their size distributions. These distributions were generated by measuring the size of ∼1000 GO sheets across several SEM images, where the characteristic size of each sheet is quantified in Figure 1 as $2\sqrt{\frac{A}{\pi}}$, where A is the measured sheet area. Figure 1 compares area-fraction *versus* size (instead of area-frequency *versus* size) because we are primarily interested in knowing the size of the sheets that predominantly contribute to the formation of the laminates. The modal sizes are ∼0.4 and ∼60 μm for Small and Large GO, respectively—an approximately 2 orders of magnitude difference.

To confirm that the sheets observed in SEM consisted of monolayer GO, we performed AFM on SiO_2 spin coated with these sheets (Figure S1). Step heights of ∼1 nm were observed for both Small and Large GO sheets, which indicates that our samples were predominantly comprised of monolayers. In some instances, the Large GO sheets were found to fold onto themselves, which increased the height to 2 nm. This measurement indicates that the interlayer spacing between two well-stacked GO monolayers is ∼1 nm, consistent with other studies in the literature.[17,34] Next, we formed Small and Large GO laminates using a custom-built dead-end filtration setup pressurized with Ar gas. Different volumes of 0.05 mg mL^{-1} dispersions of Small and Large GO sheets were filtered through nanoporous anodized aluminum oxide (AAO) membranes (13 mm in diameter) with a pore size of 20 nm. The thickness of the laminates was determined from the mass of GO filtered (concentration of GO dispersion, *i.e.*, 0.05 mg mL^{-1} × volume of solution filtered), the effective filtration area of the AAO membranes (0.75 cm^2), and the density of dehydrated GO laminates reported in literature (1.8 g cm^{-3}).[35] To verify that the thickness of the laminates was similar to theoretically predicted values, Small and Large GO laminates, obtained by filtering 100 μL of GO dispersion, were transferred from AAO membranes onto SiO_2 by etching the AAO in 5% H_3PO_4. The transferred laminates were dried for 12 h by heating at 120 °C in a N_2 atmosphere. Next, a section of the laminate was scratched with tweezers to reveal the bare underlying SiO_2, and AFM was performed across this scratched region. The measured step height of ∼40 nm for both Small and Large GO laminates (Figure S2) confirmed the expected thickness (∼36 nm). TEM indicates that both the Small and Large GO sheets are free of large tears and contain occasional wrinkles, consistent with other studies in the literature (Figure S3).[13,14]

To ascertain that the Small and Large GO sheets were chemically similar, XPS and FTIR spectroscopy were utilized.[36,37] Figure 2A shows C 1s (around 285 eV) and O 1s (around 530 eV) scans obtained from XPS spectra. The peak at ∼284 eV corresponds to C−C bonds while the peak at ∼287 eV corresponds to various C−O bonds. The peak at ∼530 eV corresponds to the total oxygen in the GO.[38] Of primary interest is the extent of oxidation (or C/O atomic ratio). This ratio can be found by integrating the total C 1s and O 1s spectral areas and correcting for the Scofield relative sensitivity factor (in this case, 2.93).[39] The measured C/O ratios for the Small and Large GO were similar, 2.5 and 2.3, respectively, in good agreement with previous studies.[36,40]

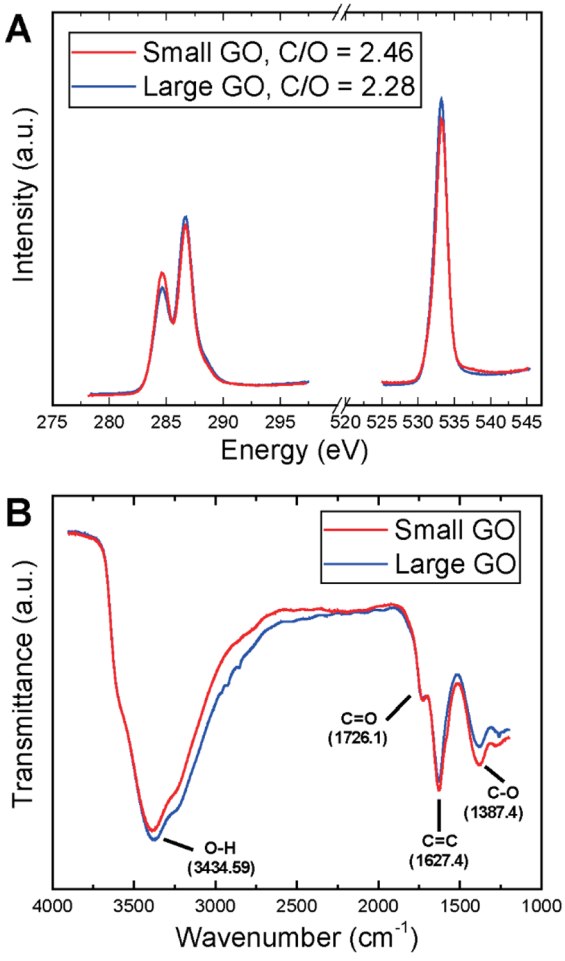

Figure 2. (A) C 1s and O 1s XPS scans of Small and Large GO laminates. (B) FTIR spectra of Small and Large GO laminates. Peaks associated with different functional groups are labeled.

To obtain more information about the functional groups and their density, we measured FTIR spectra of the laminates (Figure 2B). The features were similar in both Small and Large GO and were found to be in good agreement with several other studies in the literature.[41,42] It is worth noting that the functional groups that primarily influence the transport of water are C═C (graphitic regions) and C═O, C−O, and O−H (oxidized regions). As discussed previously, graphitic regions are believed to facilitate the nearly frictionless transport of water,[7] whereas oxidized regions are believed to impede

DOI: 10.1021/acsnano.8b02015
ACS Nano 2018, 12, 7855−7865

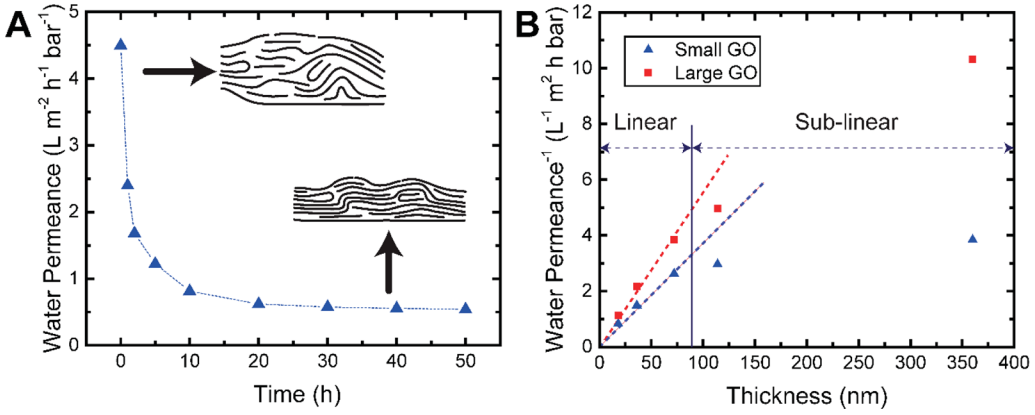

Figure 3. (A) Decay in water permeance of 36 nm thick Large GO laminate with time under an applied pressure of 5 bar. Similar behavior was observed for other thicknesses of large and Small GO laminates. (B) Inverse of steady-state water permeance of Small and Large GO laminates of various thicknesses at 5 bar. Dashed red and blue lines show expected inverse of water permeance of Small and Large GO laminates, respectively, if inverse of water permeance were to be linearly proportional to thickness. For laminate thicknesses >80 nm, linear dependence is not observed.

permeation by forming hydrogen bonds with water.[11] Therefore, a similar density of these functional groups, as evidenced by similar FTIR and XPS spectra, points toward similar in-plane water transport within Small and Large GO laminates.

Finally, the interlayer *d*-spacing of the laminates was quantified and compared using X-ray diffraction (Figure S4). The *d*-spacing for dehydrated Small and Large GO laminates was 8.75 and 8.86 Å, respectively, in good agreement with the interlayer spacing reported in several other studies.[10,43,44]

Water Permeance through Small and Large GO Laminates. Next, we measured water permeance through Small and Large GO laminates of following thicknesses: 18, 36, 72, 114, and 360 nm. For these measurements, appropriate volumes of GO solutions were first filtered through AAO membranes, as described previously. After the laminates were formed, water was loaded on top of the laminates, and pressure up to 5 bar was applied. In all experiments, the AAO membranes contributed negligible resistance to water flow, as determined by measuring the flow rate of water through bare AAO membranes, which was at least 500 times higher than through the thinnest GO laminates (~18 nm thick). The initial water permeance, depending on the thickness of the laminate, was approximately 5−10 L m^{-2} h^{-1} bar^{-1}, in agreement with previous studies.[5,22,23,44,45] As more water was passed through the laminates, the flux rapidly declined and then gradually reached a steady state (Figure 3A). This decay has been previously observed and attributed to the compaction of wrinkles and voids and increased ordering of the microstructure in the GO laminates with time.[22,23,45] Depending on the thickness of the laminate, we found that a steady state could be reached by applying continuous pressure for 1−5 days (thinner laminates reached steady state permeance sooner than thicker laminates) or by annealing the laminates at 120 °C for 30 min immediately after deposition followed by the application of continuous pressure for 1−2 days. After a steady-state had been reached, water permeance was recorded for both Small and Large GO laminates at 5 bar (Figure S6). For a particular thickness, the water permeance of the laminates was found to be invariant with pressure difference (Figure S6, inset), which indicates Darcy behavior.[44] Similar steady-state permeance values were obtained for GO laminates deposited on nanoporous polycarbonate membranes with a pore size of 80 nm, ruling out any influence of substrate on the water permeance of GO.

To confirm that our films were free of inadvertent leaks or tears that could provide a "short-cut" for water permeation, we challenged 114 nm thick laminates with 10 mL of 1.2 μg mL^{-1} solution of Evans Blue dye (EB) ($C_{34}H_{24}N_6Na_4O_{14}S_4$), which has molecular dimensions of 3.7 nm × 1.2 nm and shows maximum optical absorption at a wavelength of 600 nm.[46,47] Absorption spectra for feed, retentate, and permeate were recorded, and there was no detectable presence of EB in the permeate, which confirmed the structural integrity of the laminates (Figure S5A,B). Based on the peak absorbance values of the retentate solution, we determined that at least 81% of dye in the feed solution was rejected with less than 19% being absorbed on the surface or within the first few nanometers of the GO laminate surface. (A similar result was also observed for 36 nm thick laminates.) This observation was also confirmed by XPS depth profiling, which showed that there was no appreciable presence of nitrogen—a constituent of EB—beneath the surface of the laminate (Figure S5C,D). The water permeance of the dye solution was also found to be identical to that of deionized water, which proved that presence of dye did not influence the water transport. The Evans−Blue rejection experiments confirm that we are properly characterizing fluid transport through the GO laminates as opposed to (i) around the laminates in our filtration apparatus because of insufficient apparatus/membrane sealing or (ii) through macroscopic tears or defects that directly span the entire thickness of the entire laminates.

When the laminates are thin (<80 nm in thickness), the inverse of the water permeance—which characterizes the resistance to flow—increases linearly with laminate thickness (Figure 3B). In contrast, ref 10 has previously reported an exponential dependence for thin laminates that evolves into a linear dependence as thickness increases. Reference 10 has attributed the exponential regime to holes that extend all of the way or almost all of the away from one side of the laminate to the other due to incomplete overlap of the individual GO sheets. The linear dependence observed here indicates that our laminates are free of these trans-laminate holes, at least for laminate thicknesses >18 nm. When our laminates increase in thickness >80 nm, the inverse of the water permeance transitions to a sublinear dependence on laminate thickness.

DOI: 10.1021/acsnano.8b02015
ACS Nano 2018, 12, 7855−7865

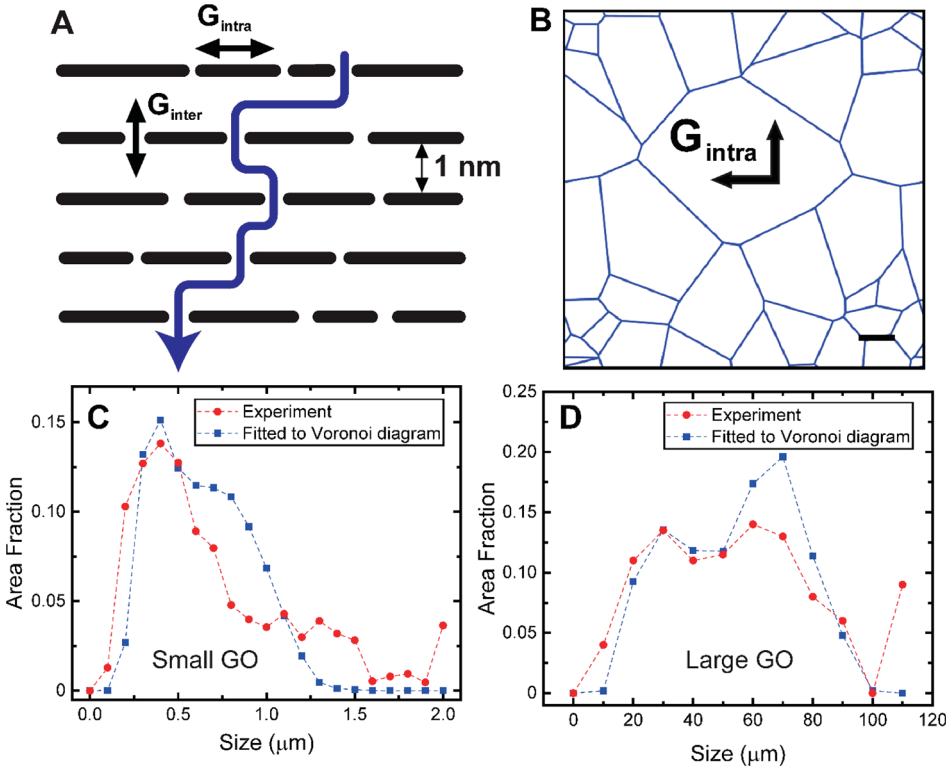

Figure 4. (A) Side view of model. Five layers of Small GO or Large GO sheets are stacked on top of each other. The blue arrow shows a transport pathway assuming there are no pinhole defects for trans-sheet flow. (B) Top view of one such Large GO layer used in the model. A Voronoi construction has been used to generate the shape and size distribution of GO sheets. Scale bar = 10 μm. (C, D) Size distributions of Small and Large GO sheets, respectively, generated by Voronoi construction *versus* experimentally observed.

The deviation from linearity for thickness >80 nm is attributed to imperfect compaction and disorder in the laminates that builds with increasing thickness and is discussed in more detail below.

Generally, the permeance through Large GO laminates was smaller than through Small GO laminates. However, analyzed over all thicknesses and pressures, the ratio of water permeance between Small and Large GO laminates varied only by a factor of 1.4−2.5. If water is assumed to travel the entire lateral dimensions of the GO sheets before progressing to the next layer, it should take longer for the water to permeate through laminates made of larger sheets than those made of smaller sheets, resulting in a permeance that decreases with increasing sheet size, which is consistent with our data. In our case, however, the Large GO sheets are about 2 orders of magnitude larger than the Small GO sheets, and thus intuitively one would expect a much larger difference in permeance. These observations cannot be explained solely by the transport of water confined in graphene nanocapillaries around the sheets.

Simulation of Water Permeance through Small and Large GO Laminates. To more quantitatively analyze the size-dependence permeation data, we simulated water flow through GO laminates, assuming layer-by-layer flow, using an interconnected nanochannel network. We constructed a finite element mesh and calculated the volumetric flow rate of water, Q_{ij}, between neighboring points i and j in the mesh as $Q_{ij} = G_{ij}\Delta P_{ij}$, where G_{ij} is a "flow conductance" that depends on the geometry of the channel, the mesh resolution, the viscosity of water, and the slip condition, and ΔP_{ij} is the pressure-difference that drives the flow. For example, in the case of no-slip boundary conditions at the walls of the channel, flow will be governed by the Newtonian Hagen−Poiseuille equation and $Q_{ij} = \frac{h^3 w \Delta P_{ij}}{12\eta L_{ij}}$, in which η is the viscosity of water, h is the channel gap (1 nm), w is the distance between mesh points normal to the direction of flow, and points i and j are separated by distance L_{ij}.[48,49] If there is slip at the boundaries then the relationship between Q_{ij} and ΔP_{ij} will still be linear if the slip length is assumed to be constant.[49] Our model does not assume any particular slip condition and therefore uses the more general $Q_{ij} = G_{ij}\Delta P_{ij}$.

Voronoi constructions[50] were used to model the microstructure of the GO laminates and to account for the polydisperse size distribution of the sheets. Figure 4A shows a side view of stacked sheets, and Figure 4B shows a top view of one such layer in our model. The sheet edges provide a pathway for water to travel from one layer to another. The size distributions of sheets generated using the Voronoi constructions match closely with the experimentally observed distributions (Figure 4C,D). Unknown in these models is the relative flow conductance within a layer (G_{intra}) compared to the flow conductance between layers (G_{inter}). The total flow conductances of the membranes were therefore modeled over a wide range of possible ratios of G_{inter} and G_{intra}. Table 1 summarizes the terms used in our model. Complete details of the model implementation can be found in the Supporting Information (Figures S8 and S9).

In Figure 5A, the ratio of the water flux through Small compared to Large GO laminates, J_{small}/J_{large}, is analyzed for different values of G_{inter}/G_{intra}, with the application of a constant pressure difference across topmost and bottom-most layers of the laminates. In this case, the sheets were assumed to

DOI: 10.1021/acsnano.8b02015
ACS Nano 2018, 12, 7855−7865

Table 1. Summary of Different Terms Used in the Model

symbol	meaning
G_{intra}	intralayer flow conductance per unit length
G_{inter}	interlayer flow conductance per unit length
G_{defect}	defect conductance
J_{small}	flux through Small GO laminate
J_{large}	flux through Large GO laminate

contain no pinholes. At very small values of G_{inter}/G_{intra}, the flux is dictated by G_{inter} and the total perimeter of the sheets. The latter is true because interlayer flow is permitted only at the edges of the sheets in the absence of defects within the sheet interiors. In this limit, J_{small}/J_{large} approaches d_{large}/d_{small}, the ratio of the sheet sizes, which is about 100.

With increasing G_{inter}/G_{intra}, G_{intra} begins to dominate and J_{small}/J_{large} increases as the longer path length for intralayer fluid flow in Large GO suppresses J_{large} more than J_{small}. An important observation from Figure 5A is that for no value of G_{inter}/G_{intra} does the flux ratio J_{small}/J_{large} approach 1. This observation clearly indicates that alternative transport mechanism(s) for flow must exist to account for the relatively small experimentally observed flux ratio of only 1.45.

In Figure 5B, J_{small}/J_{large} is analyzed considering an additional intersheet transport mechanism arising from pinhole defects within the sheet interiors. In our simulations, the pinhole defects were modeled as holes of diameter, d, of 1 nm, which provides an opening large enough to support trans-sheet water transport but small enough to block Evans Blue with molecular dimensions of ~3.7 nm × 1.2 nm.[46] The intersheet conductance through these defects, G_{defect}, was assumed to be proportional to perimeter of the pinhole multiplied by G_{inter}. Figure 5B shows that J_{small}/J_{large} decreases with increasing pinhole density, n, and approaches the regime of the experimentally measured ratio of 1.45 for n > 40000 μm^{-2}, which is one defect per 5 nm × 5 nm. In the limit of large n, the flux through the membranes is dictated by G_{defect} and becomes invariant with the lateral dimensions of the sheets. In this regime, water molecules are able to permeate between layers primarily through pinhole defects, avoiding the need to traverse the entire dimensions of individual GO sheets. One uncertainty in our model is the diameter of pinhole defects, d. However, the saturated J_{small}/J_{large} is largely insensitive to d. For example, increasing d from 0.8 to 1.2 nm yields a < 7% change in J_{small}/J_{large} for n = 40000 μm^{-2}. The density of pinhole defects predicted by our model are also consistent with HR-TEM studies,[13] which indicate pinhole defect densities of ~40000 μm^{-2} in GO sheets and pinhole sizes ranging from 0.4 to 1.9 nm with an average diameter of 1.0 nm. Therefore, pinhole defects can explain the apparent size-independence of water permeance on the lateral size of GO sheets.

IR Spectroscopy of Hydrated GO Laminates. Next, to examine the nature of the water in the GO laminates, we used infrared spectroscopy. FTIR is sensitive to the local electrostatics and hydrogen bonding environment of water.[51−53] Additionally, the width of the resonances in the spectra can be related to the distribution of microenvironments in the sample. To isolate the O−H stretch of water in a spectral region where the O−H stretches of the GO will not interfere with interpretation, we turned to the isotopically dilute O−D stretch which appears around 2500 cm^{-1}, which is free from other spectral interferences and shows identical sensitivity to hydrogen bonding and the electrostatic environment. Using dilute O−D also eliminates effects that can arise from coupling between adjacent water molecules. To incorporate dilute HOD/H_2O in GO, we placed 250 nm thick Small and Large GO laminates in a chamber and humidified (100% RH) them with 10% D_2O in H_2O for 72 h and measured FTIR spectra after hydration. GO laminates are believed to hydrate by the formation of localized pockets of water that are spatially inhomogeneous, leading to a gradual change in the interlayer spacing.[54,55] The top and bottom surfaces of the laminates were placed in contact with CaF_2 windows to prevent the condensation of water on the exterior of the laminates and to ensure that the FTIR signal originates from their interiors.

Figure 6A shows normalized FTIR spectra of the O−D stretch in hydrated Small and Large GO laminates compared to a measurement in bulk HOD/H_2O. The hydrated GO spectra are baseline corrected with the FTIR of dry GO as a reference. We observe that the OD stretch of hydrated GO laminates stays at the same frequency as bulk HOD but broadens slightly from ~167 cm^{-1} full-width-at-half-maximum (fwhm) to ~189 cm^{-1} in Small GO laminate and 194 cm^{-1} in Large GO laminate. We do not observe any shifts in the center frequency of the OD stretch for both the laminates. For the water confined primarily within the unoxidized graphene nanocapillaries, we would expect to measure an increase in the

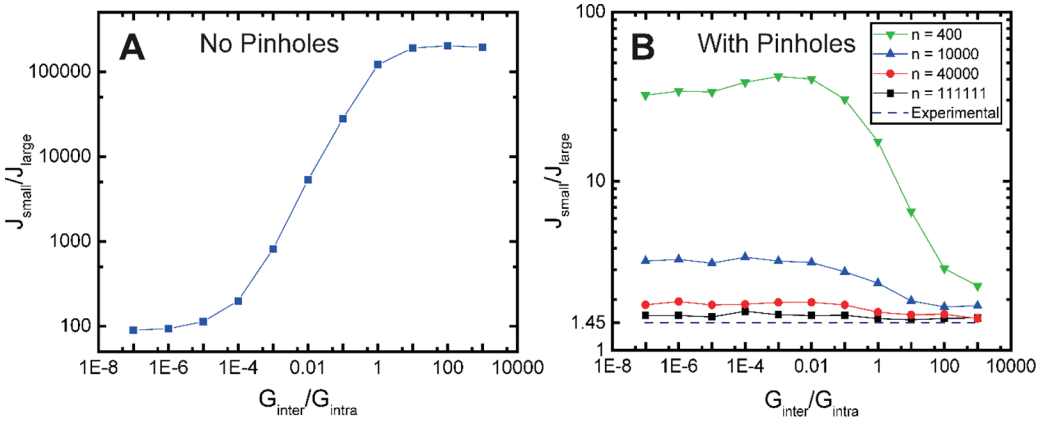

Figure 5. (A) Modeled ratios of water fluxes through Small and Large GO laminates (J_{small}/J_{large}) for different values of G_{inter}/G_{intra} in absence of pinhole defects. (B) J_{small}/J_{large} for different pinhole defect densities (n). Dashed line represents the experimentally observed flux ratio. The units of n are pinhole defects μm^{-2}.

DOI: 10.1021/acsnano.8b02015
ACS Nano 2018, 12, 7855−7865

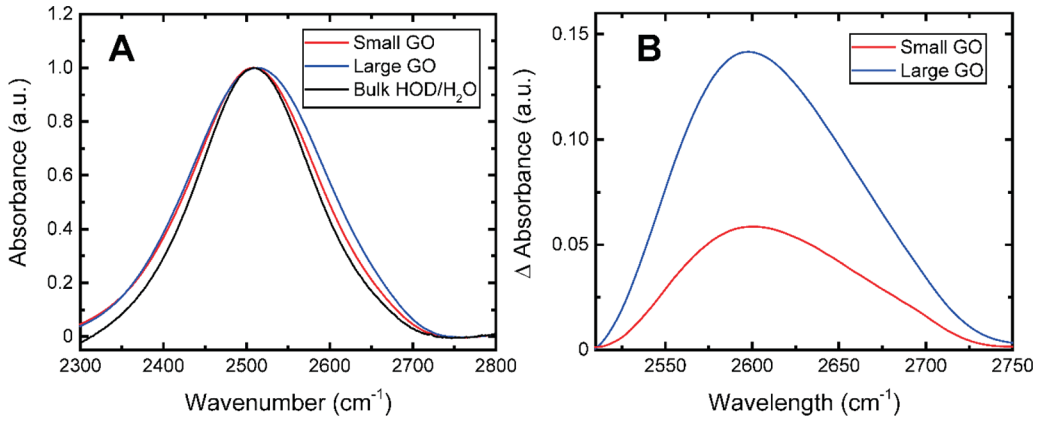

Figure 6. (A) FTIR spectra of O−D stretch of 250 nm thick Small and Large GO laminates hydrated with 10% D_2O compared to bulk 10% D_2O. (B) Small peak at 2608 cm^{-1} corresponding to confined water is observed when the bulk HOD spectrum is subtracted from HOD in the GO.

center frequency.[52,56] This is because water confined in overlapping graphitic domains has a deficient hydrogen bonding structure and therefore yields an O−D stretch at higher frequencies whereas bulk water has many partners with which it can form hydrogen bonds and thus yields O−D stretch at lower frequencies.[57] The lack of shift suggests that most of the water in our laminates contains hydrogen bonding environments that are similar to bulk water. An increase in the fwhm on the low frequency side indicates that the water is experiencing a more inhomogeneous distribution of microenvironments, which might be explained by water interacting with hydrophilic groups in GO since it is generally accepted that the frequency of the OD stretch correlates with hydrogen-bonding strength.[51]

To assign the minimal broadening on the high frequency side of the band, we subtract the bulk HOD spectrum from the spectrum of HOD in the laminates and observe a small peak at ~2608 cm^{-1} (Figure 6B). This center frequency is consistent with previous studies of water confined in reverse micelles[52,53] and, thus, is most likely from the small amount of water confined in the overlapping unoxidized graphitic domains inside the GO laminates. Observing both the small fraction of this confined water and the broadening on the low frequency side of the spectrum allows us to quantify the microenvironments of HOD in GO. Comparing the integrated areas of the peaks, we estimate that more than 89% of the water in our laminates is indistinguishable from bulk water whereas less than 7% and less than 14% of the water exists in a confined hydrophobic environment for Small and Large GO, respectively. Thus, these FTIR data suggest that even if water does exist in a confined hydrophobic environment (such as in graphene nanocapillaries) in hydrated GO laminates then the abundance of this confined water is very small.

The FTIR spectra, alone, do not indicate where in the GO laminates that the bulk-like water resides. This liquid-like water may be (i) intercalated between individual GO sheets within the laminates and/or (ii) reside within wrinkles and voids. Regarding (i), Talyzin *et al.*[58] have reported that about half of the total water intercalated inside the GO laminates under ambient conditions exhibits bulk-like behavior. Prior XRD studies have also failed to identify a crystalline phase of water in GO, indicating that it is liquid-like.[59] The pseudonegative thermal expansion of GO as observed by Zhu *et al.*[60] likewise suggests that a majority of water in hydrated GO laminates is bulk-like or interacting with the hydrophilic functional groups. The relatively broad interlayer *d*-spacing scattering peaks that are observed in the X-ray diffraction spectra of hydrated GO laminates also suggest that the water that is intercalated between individual sheets in GO laminates is disorderd.[61,62] Regarding (ii), cross-sectional imaging has revealed the presence of noninterlamellar voids and wrinkles in GO laminates (see the Discussion). Moreover, neutron-scattering studies of GO laminates at high hydration levels have revealed the presence of bulk-like water that resides in these voids and wrinkles.[54,63]

DISCUSSION

The mechanism for water transport through GO laminates is dependent on the extent of oxidation (C/O ratio), size of the nanosheets,[22] and stacking of nanosheets.[64] Based on our experiments and simulations, we believe that water transport through GO laminates occurs primarily by two pathways: (a) pinhole defects, that circumvent the need for water to travel the entire lateral dimension of individual sheets and/or (b) flow through regions arising from imperfect stacking in the laminates.

The presence of pinhole defects can reduce the effective path length that water needs to travel laterally before permeating between the layers (Figure 7B). Pinhole defects are known to form during the synthesis of GO by the Hummers method.[65] Such pinholes are believed to cause selective permeation of H_2 through GO laminates[19] and have been observed by direct imaging by HR-TEM.[13] If water is assumed to flow strictly between the sheets, our simulations predict that pinhole defects must exist to explain the apparent indifference of water permeance on the lateral size of GO nanosheets. The density of pinhole defects predicted by our simulations are also consistent with those observed in HR-TEM studies.

Deposition technique also plays an important role in determining the microstructure and consequently the sieving properties of GO laminates.[18,66] In an ideal stack of GO nanosheets, where water follows a tortuous path between individual nanosheets (Figure 7A), the water permeance would be expected to vary inversely with laminate thickness and decrease with increasing sheet size. Practically, however, the ideal lamellar stacking of sheets is unlikely to happen during pressure assisted deposition because the sheets are randomly

DOI: 10.1021/acsnano.8b02015
ACS Nano 2018, 12, 7855−7865

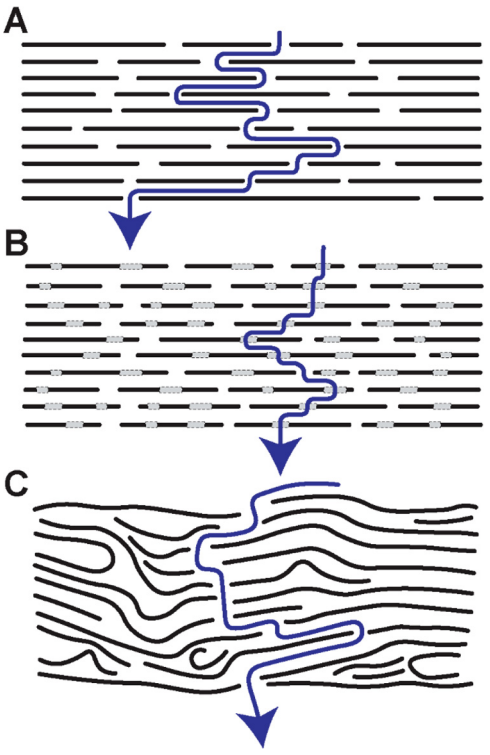

Figure 7. Possible water-transport mechanisms through GO laminates. (A) Layer-by-layer water transport in which water flows strictly between the individual GO sheets. (B) Layer-by-layer transport, mediated by pinhole defects, in which the effective path length is significantly reduced by the pinhole defects. (C) Combination of layer-by-layer transport and transport mediated by voids and imperfect sheet stacking.

oriented in the solution. Often a sheet might fold onto itself, aggregate with other sheets, or form wrinkles and voids (Figure 7C). These features have been experimentally observed in GO laminates. Recently, Nandy *et al.*[67] observed a hierarchical structure within GO laminates, where tens of GO sheets stack by ordering into "lamellae" that are ~25 nm thick (primary structure) and groups of lamellae form "superlamellae" (secondary structure). The secondary structure or "superlamellae" are less compacted and therefore the space in between the "superlamellae" likely yields voids that allow for shorter pathways for water transport. This effect is more profound in thick GO laminates.[22] This loosely compacted structure of GO laminates may also accommodate "bulk-water" comprising of several monolayers of water. Thus, water no longer has to flow through a tortuous pathway between individual GO sheets—as might be expected in the ideal scenario. When compressed for a long time, the microstructure of the laminate becomes more ordered and some of these pathways close (*e.g.*, superlamellae become compacted) leading to a lower water permeance. This is consistent with the time-dependent decay of water permeance observed in our laminates that is independent of sheet size. Moreover, for a given pressure difference, a much higher compaction will be achieved in thin laminates compared to thick laminates, as the pressure drop per layer is larger in thin laminates. This explains the deviation from the inverse permeance dependence on laminate thickness as the thickness of the laminates increases (Figure 3B). Voids in GO laminates can occur either due to incomplete compression of the sheets leading to formation of wrinkles[45] or empty spaces created due to nonoverlapping sheets, as proposed by Yang *et al.*[10] We speculate that such voids are rather localized and not interconnected through the entire thickness of the laminate, as we did not observe any detectable dye beyond the surface of the laminate. Therefore, at larger thicknesses, while transport in the interstitial regions between layers is still the rate limiting step, the presence of voids reduces the necessity to travel through the entire thickness of the laminate, layer-by-layer, and rather creates additional pathways of lower resistance. In other words, at larger thicknesses, there are fewer interstitial transport events per unit thickness, which decreases the resistance to flow per unit thickness. The presence of such voids is also consistent with our FTIR spectra of hydrated GO laminates, which shows predominantly bulk-like water, although the bulk-like water signatures may also originate from well-ordered lamellar regions that accommodate multiple layers of water between each sheet.

CONCLUSION

In this study, we synthesized graphene oxide (GO) sheets with vastly different sizes but with similar chemical composition. We fabricated laminates of different thicknesses from these sheets and compared the water permeance. Even though the lateral dimensions of the sheets varied by a factor of 100, the water permeance varied by only a factor of 1.45−2.5. We then simulated fluid flow through these laminates using an interconnected nanochannel network model. The experimental observation that water permeance is relatively invariant with sheet size can only be reproduced in simulations if pinhole defects are introduced into the GO sheets that permit trans-sheet flow. An alternative explanation is that the flow of water is not always perfectly confined between the sheets—presumably due to presence of disordered sheet packing and voids. In contrast, in the absence of such nonidealities, water would need to travel the entire lateral dimensions of the sheets, resulting in a much larger difference in permeation rate. In the absence of pinhole defects and voids, the simulations specifically predict that the smallest possible difference in permeation rate will be dictated by the difference in the lateral dimensions of the sheets—in this case a factor of 100, significantly exceeding the experimentally observed difference. Thus, both the experiments and simulations reported here are consistent with several other reports in the literature which attribute the predominant pathway of water transport in GO laminates to presence of pinhole defects in the sheets and/or voids inside the laminates,[11−13] contradicting the circuitous pathway/nanocapillary model.

Finally, by comparing FTIR spectra of water in GO laminates *versus* in bulk solution, we show that water in GO laminates predominantly experiences an electrostatic environment similar to that of the bulk. Our experimental results in tandem with simulations provide useful insights into the transport mechanisms and nature of water inside GO laminates. These insights can potentially guide the design of next-generation GO membranes with improved performance in terms of enhanced permeability and salt rejection.

METHODS

Materials. Graphite flakes were purchased from Sigma-Aldrich (product no. 332461), H_2SO_4 from Fisher Scientific (lot no. 167437), $KMnO_4$ from Amresco (lot no. 1583C380), and H_2O_2 from Fisher Scientific (lot no. 167306). AAO membranes were purchased from

DOI: 10.1021/acsnano.8b02015
ACS Nano 2018, 12, 7855−7865

GE Healthcare Life Sciences (product no. 6809-5502, pore size = 20 nm). Evans blue dye was purchased from Sigma-Aldrich (product no. E2129-10G, lot no. MKBX1555 V). D_2O was purchased from Sigma-Aldrich (product no. 151882).

GO Synthesis. For Small GO, 1 g of graphite was dispersed in 98% H_2SO_4 in a 250 mL flask kept in an ice bath. A magnetic stirrer was used for 30 min to aid in the intercalation of the graphite. Then, 4 g of $KMnO_4$ was slowly added and stirred for an additional 10 min. The flask was next transferred from the ice bath to a water bath heated at 40 °C. The whole mixture was stirred vigorously for 1 h. Then, 100 mL of deionized water was added to the mixture under constant stirring, and the whole mixture was heated at 95 °C for 15 min. The mixture was then poured into a 1:10 v/v mixture of H_2O_2/H_2O and kept for 12 h. Subsequently, the pellets were collected and poured into 12 mL centrifuge tubes and centrifuged in a swing bucket rotor (Sorvall WX, TH-641, Thermo Scientific) at 4000 rpm until the supernatant was clear. The supernatant was collected and pellets were redispersed in 10% v/v HCl in water. We call this procedure as one washing step. Several washing steps were needed to reach a constant pH value. In our experiments, we stopped when three subsequent washing steps yielded the same pH value. In this case, we stopped at pH = 5.5.

For Large GO, we replicated the synthesis procedure used by Dimiev *et al.*[26] To describe briefly, 6 g of graphite was dispersed in 98% H_2SO_4 at room temperature using a magnetic stirrer. After 15 min of stirring, $KMnO_4$ was added. The mixture turned green due to the formation of the oxidizing agent MnO_3^+. After 1 day, the green color disappeared, indicating the complete consumption of MnO_3^+. Six grams of $KMnO_4$ was added for the next 3 days to completely oxidize the graphite. Next, this oxidized mixture was quenched in an ice bath, and a few drops of 30% H_2O_2 were added until the solution turned light yellow. This solution was then centrifuged at 4100 rpm and washed with deionized water. These centrifuge-washing cycles were repeated until the supernatant reached a constant pH value (~5.5) and the pellets turned yellowish brown. The pellets after the final stage of washing were dried to yield the GO powder.

X-ray Photoelectron Spectroscopy. The XPS spectra were measured using a Thermo K-Alpha XPS with an X-ray spot size of 400 μm and monochromatic Al Kα radiation (1486.7 eV). Survey and individual spectra were acquired using analyzer pass energies of 188 and 50 eV, respectively.

Fourier Transform Infrared Spectroscopy. The FTIR spectra were collected with a Nicolet iS10 FTIR spectrometer (Thermo) adapted with a beam condenser (Pike Technologies). Each spectrum reported is an average of 500 scans with 1 cm^{-1} resolution. The spectrometer is purged with dry air to remove contributions from water vapor and CO_2.

ASSOCIATED CONTENT

Supporting Information

The Supporting Information is available free of charge on the ACS Publications website at DOI: 10.1021/acsnano.8b02015.

AFM of Small and Large GO sheets (Figure S1) and 40 nm thick GO laminates (Figure S2); TEM of single-layered GO sheets (Figure S3); XRD of 100 nm thick GO laminates (Figure S4); dye challenges (Figure S5); thickness- and pressure-dependent water permeance of GO laminates (Figure S6); quantification of sulfur contamination in GO laminates (Figure S7, Tables S1 and S2), and description of implementation of interconnected nanochannel network model (Figures S8 and S9) (PDF)

AUTHOR INFORMATION

Corresponding Author

*E-mail: michael.arnold@wisc.edu.

ORCID

Vivek Saraswat: 0000-0001-5095-3078
Robert M. Jacobberger: 0000-0001-5947-5308
Joshua S. Ostrander: 0000-0002-6338-6639
Austin J. Way: 0000-0002-7418-8590
Martin T. Zanni: 0000-0001-7191-9768
Michael S. Arnold: 0000-0002-2946-5480

Notes

The authors declare no competing financial interest.

ACKNOWLEDGMENTS

V.S., C.L.H., J.W., and M.S.A. acknowledge initial support from the National Science Foundation through the University of Wisconsin—Madison Center of Excellence for Materials Research and Innovation Award No. DMR-1121288 and then later support from National Science Foundation Award No. CBET-1705503 for GO synthesis and characterization, measurement of permeance, and modeling. R.M.J. and A.J.W. acknowledge support from the U.S. Department of Energy, Office of Science, Basic Energy Sciences, under Award No. DE-SC0016007 for XPS analysis of graphene oxide and design of the dead-end filtration apparatus. M.T.Z. acknowledges the Air Force Office of Scientific Research (FA9550-15-1-0061) for support. A.J.W. also acknowledges support from NSF Graduate Research Fellowship Grant No. DGE-1256259.

REFERENCES

(1) Huang, K.; Liu, G.; Lou, Y.; Dong, Z.; Shen, J.; Jin, W. A Graphene Oxide Membrane with Highly Selective Molecular Separation of Aqueous Organic Solution. *Angew. Chem., Int. Ed.* **2014**, *53*, 6929−6932.

(2) Shen, J.; Liu, G.; Huang, K.; Chu, Z. Y.; Jin, W.; Xu, N. Subnanometer Two-Dimensional Graphene Oxide Channels for Ultrafast Gas Sieving. *ACS Nano* **2016**, *10*, 3398−3409.

(3) Li, D.; Müller, M. B.; Gilje, S.; Kaner, R. B.; Wallace, G. G. Processable Aqueous Dispersions of Graphene Nanosheets. *Nat. Nanotechnol.* **2008**, *3*, 101−105.

(4) Abraham, J.; Vasu, K. S.; Williams, C. D.; Gopinadhan, K.; Su, Y.; Cherian, C. T.; Dix, J.; Prestat, E.; Haigh, S. J.; Grigorieva, I. V.; Carbone, P.; Geim, A. K.; Nair, R. R. Tunable Sieving of Ions Using Graphene Oxide Membranes. *Nat. Nanotechnol.* **2017**, *12*, 546−550.

(5) Han, Y.; Xu, Z.; Gao, C. Ultrathin Graphene Nanofiltration Membrane for Water Purification. *Adv. Funct. Mater.* **2013**, *23*, 3693−3700.

(6) Hu, M.; Mi, B. Enabling Graphene Oxide Nanosheets as Water Separation Membranes. *Environ. Sci. Technol.* **2013**, *47*, 3715−3723.

(7) Nair, R. R.; Wu, H. A.; Jayaram, P. N.; Grigorieva, I. V.; Geim, A. K. Unimpeded Permeation of Water Through Helium-Leak-Tight Graphene-Based Membranes. *Science* **2012**, *335*, 442−444.

(8) Joshi, R. K.; Carbone, P.; Wang, F. C.; Kravets, V. G.; Su, Y.; Grigorieva, I. V.; Wu, H. A.; Geim, A. K.; Nair, R. R. Precise and Ultrafast Molecular Sieving Through Graphene Oxide Membranes. *Science* **2014**, *343*, 752−754.

(9) Mi, B. Graphene Oxide Membranes for Ionic and Molecular Sieving. *Science* **2014**, *343*, 740−742.

(10) Yang, Q.; Su, Y.; Chi, C.; Cherian, C. T.; Huang, K.; Kravets, V. G.; Wang, F. C.; Zhang, J. C.; Pratt, A.; Grigorenko, A. N.; Guinea, F.; Geim, A. K.; Nair, R. R. Ultrathin Graphene-Based Membrane with Precise Molecular Sieving and Ultrafast Solvent Permeation. *Nat. Mater.* **2017**, *16*, 1198−1202.

(11) Devanathan, R.; Chase-Woods, D.; Shin, Y.; Gotthold, D. W. Molecular Dynamics Simulations Reveal that Water Diffusion between Graphene Oxide Layers is Slow. *Sci. Rep.* **2016**, *6*, 29484.

DOI: 10.1021/acsnano.8b02015
ACS Nano 2018, 12, 7855−7865

(12) Talyzin, A. V.; Hausmaninger, T.; You, S.; Szabo, T. The Structure of Graphene Oxide Membranes in Liquid Water, Ethanol and Water-Ethanol Mixtures. *Nanoscale* **2014**, *6*, 272−281.
(13) Erickson, K.; Erni, R.; Lee, Z.; Alem, N.; Gannett, W.; Zettl, A. Determination of the Local Chemical Structure of Graphene Oxide and Reduced Graphene Oxide. *Adv. Mater.* **2010**, *22*, 4467−4472.
(14) Dave, S. H.; Gong, C.; Robertson, A. W.; Warner, J. H.; Grossman, J. C. Chemistry and Structure of Graphene Oxide *via* Direct Imaging. *ACS Nano* **2016**, *10*, 7515−7522.
(15) Loh, K. P.; Bao, Q.; Eda, G.; Chhowalla, M. Graphene Oxide As a Chemically Tunable Platform for Optical Applications. *Nat. Chem.* **2010**, *2*, 1015−1024.
(16) Mattevi, C.; Eda, G.; Agnoli, S.; Miller, S.; Mkhoyan, K. A.; Celik, O.; Mastrogiovanni, D.; Granozzi, G.; Garfunkel, E.; Chhowalla, M. Evolution of Electrical, Chemical, and Structural Properties of Transparent and Conducting Chemically Derived Graphene Thin Films. *Adv. Funct. Mater.* **2009**, *19*, 2577−2583.
(17) Si, Y.; Samulski, E. T. Synthesis of Water Soluble Graphene. *Nano Lett.* **2008**, *8*, 1679−1682.
(18) Kim, H. W.; Yoon, H. W.; Yoon, S. M.; Yoo, B. M.; Ahn, B. K.; Cho, Y. H.; Shin, H. J.; Yang, H.; Paik, U.; Kwon, S.; Choi, J. Y.; Park, H. B. Selective Gas Transport Through Few-Layered Graphene and Graphene Oxide Membranes. *Science* **2013**, *342*, 91−95.
(19) Li, H.; Song, Z.; Zhang, X.; Huang, Y.; Li, S.; Mao, Y.; Ploehn, H. J.; Bao, Y.; Yu, M. Ultrathin, Molecular-Sieving Graphene Oxide Membranes for Selective Hydrogen Separation. *Science* **2013**, *342*, 95−98.
(20) Wei, N.; Peng, X.; Xu, Z. Understanding Water Permeation in Graphene Oxide Membranes. *ACS Appl. Mater. Interfaces* **2014**, *6*, 5877−5883.
(21) Gómez-Navarro, C.; Meyer, J. C.; Sundaram, R. S.; Chuvilin, A.; Kurasch, S.; Burghard, M.; Kern, K.; Kaiser, U. Atomic Structure of Reduced Graphene Oxide. *Nano Lett.* **2010**, *10*, 1144−1148.
(22) Chong, J. Y.; Wang, B.; Mattevi, C.; Li, K. Dynamic Microstructure of Graphene Oxide Membranes and the Permeation Flux. *J. Membr. Sci.* **2018**, *549*, 385−392.
(23) Cho, Y. H.; Kim, H. W.; Lee, H. D.; Shin, J. E.; Yoo, B. M.; Park, H. B. Water and Ion Sorption, Diffusion, and Transport in Graphene Oxide Membranes Revisited. *J. Membr. Sci.* **2017**, *544*, 425−435.
(24) Hummers, W. S.; Offeman, R. E. Preparation of Graphitic Oxide. *J. Am. Chem. Soc.* **1958**, *80*, 1339−1339.
(25) Marcano, D. C.; Kosynkin, D. V.; Berlin, J. M.; Sinitskii, A.; Sun, Z.; Slesarev, A.; Alemany, L. B.; Lu, W.; Tour, J. M. Improved Synthesis of Graphene Oxide. *ACS Nano* **2010**, *4*, 4806−4814.
(26) Dimiev, A. M.; Alemany, L. B.; Tour, J. M. Graphene Oxide. Origin of Acidity, Its Instability in Water, and a New Dynamic Structural Model. *ACS Nano* **2013**, *7*, 576−588.
(27) Dimiev, A. M.; Tour, J. M. Mechanism of Graphene Oxide Formation. *ACS Nano* **2014**, *8*, 3060−3068.
(28) Dreyer, D. R.; Park, S.; Bielawski, C. W.; Ruoff, R. S. The Chemistry of Graphene Oxide. *Chem. Soc. Rev.* **2010**, *39*, 228−240.
(29) Compton, O. C.; Nguyen, S. T. Graphene Oxide, Highly Reduced Graphene Oxide, and Graphene: Versatile Building Blocks for Carbon-Based Materials. *Small* **2010**, *6*, 711−723.
(30) Lerf, A.; He, H.; Forster, M.; Klinowski, J. Structure of Graphite Oxide Revisited. *J. Phys. Chem. B* **1998**, *102*, 4477−4482.
(31) He, H.; Klinowski, J.; Forster, M.; Lerf, A. A New Structural Model for Graphite Oxide. *Chem. Phys. Lett.* **1998**, *287*, 53−56.
(32) Gambhir, S.; Jalili, R.; Officer, D. L.; Wallace, G. G. Chemically Converted Graphene: Scalable Chemistries to Enable Processing and Fabrication. *NPG Asia Mater.* **2015**, *7*, e186.
(33) Qi, X.; Zhou, T.; Deng, S.; Zong, G.; Yao, X.; Fu, Q. Size-Specified Graphene Oxide Sheets: Ultrasonication Assisted Preparation and Characterization. *J. Mater. Sci.* **2014**, *49*, 1785−1793.
(34) Paredes, J. I.; Villar-Rodil, S.; Solis-Fernandez, P.; Martinez-Alonso, A.; Tascon, J. M. D. Atomic Force and Scanning Tunneling Microscopy Imaging of Graphene Nanosheets Derived from Graphite Oxide. *Langmuir* **2009**, *25*, 5957−5968.
(35) Dikin, D. A.; Stankovich, S.; Zimney, E. J.; Piner, R. D.; Dommett, G. H. B.; Evmenenko, G.; Nguyen, S. T.; Ruoff, R. S. Preparation and Characterization of Graphene Oxide Paper. *Nature* **2007**, *448*, 457−460.
(36) Yang, D.; Velamakanni, A.; Bozoklu, G.; Park, S.; Stoller, M.; Piner, R. D.; Stankovich, S.; Jung, I.; Field, D. A.; Ventrice, C. A.; Ruoff, R. S. Chemical Analysis of Graphene Oxide Films After Heat and Chemical Treatments by X-Ray Photoelectron and Micro-Raman Spectroscopy. *Carbon* **2009**, *47*, 145−152.
(37) Eda, G.; Fanchini, G.; Chhowalla, M. Large-Area Ultrathin Films of Reduced Graphene Oxide as a Transparent and Flexible Electronic Material. *Nat. Nanotechnol.* **2008**, *3*, 270−274.
(38) Datsyuk, V.; Kalyva, M.; Papagelis, K.; Parthenios, J.; Tasis, D.; Siokou, A.; Kallitsis, I.; Galiotis, C. Chemical Oxidation of Multiwalled Carbon Nanotubes. *Carbon* **2008**, *46*, 833−840.
(39) Kim, S.; Zhou, S.; Hu, Y.; Acik, M.; Chabal, Y. J.; Berger, C.; de Heer, W.; Bongiorno, A.; Riedo, E. Room-Temperature Metastability of Multilayer Graphene Oxide Films. *Nat. Mater.* **2012**, *11*, 544−549.
(40) Li, X. L.; Wang, H. L.; Robinson, J. T.; Sanchez, H.; Diankov, G.; Dai, H. J. Simultaneous Nitrogen Doping and Reduction of Graphene Oxide. *J. Am. Chem. Soc.* **2009**, *131*, 15939−15944.
(41) Sudesh; Kumar, N.; Das, S.; Bernhard, C.; Varma, G. D. Effect of Graphene Oxide Doping on Superconducting Properties of Bulk MgB_2. *Supercond. Sci. Technol.* **2013**, *26*, 095008.
(42) Acik, M.; Lee, G.; Mattevi, C.; Chhowalla, M.; Cho, K.; Chabal, Y. J. Unusual Infrared-Absorption Mechanism in Thermally Reduced Graphene Oxide. *Nat. Mater.* **2010**, *9*, 840−845.
(43) Lin, X.; Shen, X.; Zheng, Q.; Yousefi, N.; Ye, L.; Mai, Y. W.; Kim, J. K. Fabrication of Highly-Aligned, Conductive, and Strong Graphene Papers Using Ultra Large Graphene Oxide Sheets. *ACS Nano* **2012**, *6*, 10708−10719.
(44) Amadei, C. A.; Montessori, A.; Kadow, J. P.; Succi, S.; Vecitis, C. D. Role of Oxygen Functionalities in Graphene Oxide Architectural Laminate Subnanometer Spacing and Water Transport. *Environ. Sci. Technol.* **2017**, *51*, 4280−4288.
(45) Wei, Y.; Zhang, Y.; Gao, X.; Yuan, Y.; Su, B.; Gao, C. Declining Flux and Narrowing Nanochannels Under Wrinkles of Compacted Graphene Oxide Nanofiltration Membranes. *Carbon* **2016**, *108*, 568−575.
(46) Huang, H.; Song, Z.; Wei, N.; Shi, L.; Mao, Y.; Ying, Y.; Sun, L.; Xu, Z.; Peng, X. Ultrafast Viscous Water Flow Through Nanostrand-Channelled Graphene Oxide Membranes. *Nat. Commun.* **2013**, *4*, 2979.
(47) An, D.; Yang, L.; Wang, T. J.; Liu, B. Separation Performance of Graphene Oxide Membrane in Aqueous Solution. *Ind. Eng. Chem. Res.* **2016**, *55*, 4803−4810.
(48) Akbari, A.; Sheath, P.; Martin, S. T.; Shinde, D. B.; Shaibani, M.; Banerjee, P. C.; Tkacz, R.; Bhattacharyya, D.; Majumder, M. Large-Area Graphene-Based Nanofiltration Membranes by Shear Alignment of Discotic Nematic Liquid Crystals of Graphene Oxide. *Nat. Commun.* **2016**, *7*, 10891.
(49) Li, L.; Mo, J.; Li, Z. Flow and Slip Transition in Nanochannels. *Phys. Rev. E* **2014**, *90*, 033003.
(50) Brostow, W.; Dussault, J. P.; Fox, B. L. Construction of Voronoi Polyhedra. *J. Comput. Phys.* **1978**, *29*, 81−92.
(51) Bakker, H. J.; Skinner, J. L. Vibrational Spectroscopy as a Probe of Structure and Dynamics in Liquid Water. *Chem. Rev.* **2010**, *110*, 1498−1517.
(52) Fayer, M. D.; Levinger, N. E. Analysis of Water in Confined Geometries and at Interfaces. *Annu. Rev. Anal. Chem.* **2010**, *3*, 89−107.
(53) Fayer, M. D. Dynamics of Water Interacting with Interfaces, Molecules, and Ions. *Acc. Chem. Res.* **2012**, *45*, 3−14.
(54) Lerf, A.; Buchsteiner, A.; Pieper, J.; Schöttl, S.; Dekany, I.; Szabo, T.; Boehm, H. P. Hydration Behavior and Dynamics of Water Molecules in Graphite Oxide. *J. Phys. Chem. Solids* **2006**, *67*, 1106−1110.
(55) Rezania, B.; Severin, N.; Talyzin, A. V.; Rabe, J. P. Hydration of Bilayered Graphene Oxide. *Nano Lett.* **2014**, *14*, 3993−3998.

DOI: 10.1021/acsnano.8b02015
ACS Nano 2018, 12, 7855−7865

(56) Tan, H. S.; Piletic, I. R.; Riter, R. E.; Levinger, N. E.; Fayer, M. D. Dynamics of Water Confined on a Nanometer Length Scale in Reverse Micelles: Ultrafast Infrared Vibrational Echo Spectroscopy. *Phys. Rev. Lett.* **2005**, *94*, 057405.
(57) Tabor, D. P.; Kusaka, R.; Walsh, P. S.; Sibert, E. L., III; Zwier, T. S. Isomer-Specific Spectroscopy of Benzene-$(H_2O)_n$, n = 6,7: Benzene's Role in Reshaping Water's Three-Dimensional Networks. *J. Phys. Chem. Lett.* **2015**, *6*, 1989−1995.
(58) Talyzin, A. V.; Luzan, S. M.; Szabo, T.; Chernyshev, D.; Dmitriev, V. Temperature Dependent Structural Breathing of Hydrated Graphite Oxide in H_2O. *Carbon* **2011**, *49*, 1894−1899.
(59) Talyzin, A. V.; Solozhenko, V. L.; Kurakevych, O. O.; Szabo, T.; Dekany, I.; Kurnosov, A.; Dmitriev, V. Colossal Pressure-Induced Lattice Expansion of Graphite Oxide in the Presence of Water. *Angew. Chem., Int. Ed.* **2008**, *47*, 8268−8271.
(60) Zhu, J.; Andres, C. M.; Xu, J.; Ramamoorthy, A.; Tsotsis, T.; Kotov, N. A. Pseudonegative Thermal Expansion and the State of Water in Graphene Oxide Layered Assemblies. *ACS Nano* **2012**, *6*, 8357−8365.
(61) Barroso-Bujans, F.; Cerveny, S.; Alegria, A.; Colmenero, J. Sorption and Desorption Behavior of Water and Organic Solvents from Graphite Oxide. *Carbon* **2010**, *48*, 3277−3286.
(62) Zheng, S.; Tu, Q.; Urban, J. J.; Li, S.; Mi, B. Swelling of Graphene Oxide Membranes in Aqueous Solution: Characterization of Interlayer Spacing and Insight into Water Transport Mechanisms. *ACS Nano* **2017**, *11*, 6440−6450.
(63) Buchsteiner, A.; Lerf, A.; Pieper, J. Water Dynamics in Graphite Oxide Investigated with Neutron Scattering. *J. Phys. Chem. B* **2006**, *110*, 22328−22338.
(64) Xu, W. L.; Fang, C.; Zhou, F.; Song, Z.; Liu, Q.; Qiao, R.; Yu, M. Self-Assembly: A Facile Way of Forming Ultrathin, High-Performance Graphene Oxide Membranes for Water Purification. *Nano Lett.* **2017**, *17*, 2928−2933.
(65) Eigler, S.; Hirsch, A. Chemistry with Graphene and Graphene Oxide-Challenges for Synthetic Chemists. *Angew. Chem., Int. Ed.* **2014**, *53*, 7720−7738.
(66) Tsou, C. H.; An, Q. F.; Lo, S. C.; De Guzman, M.; Hung, W. S.; Hu, C. C.; Lee, K. R.; Lai, J. Y. Effect of Microstructure of Graphene Oxide Fabricated through Different Self-Assembly Techniques on 1-butanol Dehydration. *J. Membr. Sci.* **2015**, *477*, 93−100.
(67) Nandy, K.; Palmeri, M. J.; Burke, C. M.; An, Z.; Nguyen, S. T.; Putz, K. W.; Brinson, L. C. Stop Motion Animation Reveals Formation Mechanism of Hierarchical Structure in Graphene Oxide Papers. *Adv. Mater. Interfaces* **2016**, *3*, 1500666.

DOI: 10.1021/acsnano.8b02015
ACS Nano 2018, 12, 7855−7865